



# Periodic Eigendecomposition and Its Application to Kuramoto–Sivashinsky Kuramoto–Sivashinsky System\*

Xiong Ding<sup>†</sup> and Predrag Cvitanović<sup>†</sup>

**Abstract.** Periodic eigendecomposition, to be formulated in this paper, is a numerical method to compute Floquet spectrum and Floquet vectors along periodic orbits in a dynamical system. It is rooted in numerical algorithm advances in computation of covariant Lyapunov vectors of the linearized flow along an ergodic trajectory in a chaotic system. Also, we incorporate periodic Schur decomposition to the computation of Floquet vectors, compare it with other methods, and show that periodic eigendecomposition can yield the full set of Floquet vectors of a periodic orbit at every point along the orbit to high accuracy. Its power, and in particular its ability to resolve eigenvalues differing by hundreds of orders of magnitude, is demonstrated by applying the algorithm to computation of the full linear stability spectrum of several periodic solutions in one-dimensional Kuramoto–Sivashinsky flow.

**Key words.** periodic eigendecomposition, periodic Schur decomposition, periodic Sylvester equation, covariant Lyapunov vectors, Floquet vectors, Kuramoto–Sivashinsky, linear stability, continuous symmetry

**AMS subject classifications.** 15A18, 35B10, 37L20, 37M25, 65F15, 65H10, 65P20, 65P40, 76F20

**DOI.** 10.1137/15M1037299

**1. Introduction.** In dissipative chaotic dynamical systems, the decomposition of the tangent space of invariant subsets into stable, unstable, and center subspaces is important for analyzing the geometrical structure of the solution field [17]. For equilibrium states, the task is quite simple, which, it is reduced to the eigen-problem eigenproblem of a single stability matrix, but the scenario is much more difficult for complex structures, such as periodic orbits and invariant tori, since the expansion/contraction rates in high-dimensional-high-dimensional systems usually span a large range of orders of magnitude. Actually, in the literature, two different algorithms are capable of resolving this problem partially originated from different settings. The first candidate is the covariant Lyapunov vector algorithm [13, 14, 21, 34]. It is designed to stratify the Oseledets subspaces [25, 26] corresponding to the hierarchy of Lyapunov exponents along a long nonwandering orbit on the attractor. Covariant Lyapunov vectors attract have attracted a lot of attention in the past few years. They turn have turned out to be a useful tool for physicists to investigate the dynamical properties of the system, such as the hyperbolicity degree [4, 18, 20] and the geometry of the inertial manifold [27, 35, 37]. For our interest in periodic orbits, it, covariant Lyapunov vector algorithm produces Floquet spectrum and Floquet vectors. The second candidate is periodic Schur decomposition

\*Received by the editors August 28, 2015; accepted for publication (in revised form) by D. Barkley May 19, 2016; published electronically DATE.

<http://www.siam.org/journals/siads/x-x/M103729.html>

<sup>†</sup>Center for Nonlinear Science, School of Physics, Georgia Institute of Technology, Atlanta, GA 30332 (xding@gatech.edu, predrag.cvitanovic@physics.gatech.edu). The research of the first author was supported by NSF grant DMS-1028133.

(PSD) [3, 32], which ~~was~~ brought up to compute the eigenvalues of the product of a sequence of matrices without forming the product explicitly. This is suitable for solving the eigenvalue problem in tangent space because the fundamental matrix in tangent space can be formed as a product of its shorter-time pieces. However, in its original form, PSD is ~~only~~-capable of computing only eigenvalues but not eigenvectors. Also, PSD ~~seems not~~ does not seem to be well known to the physics community.

In this paper, we unify these two methods for computing Floquet spectrum and Floquet vectors along periodic orbits or invariant tori, and ~~use~~ use it after *periodic eigendecomposition*. Special attention is ~~exerted~~ given to complex conjugate Floquet vectors. There are two stages in the process of this algorithm, each of which can be accomplished by two different methods, so we study the performance of four different algorithms in all. Also, it turns out that the covariant Lyapunov vector algorithm reduces to one of ~~them~~ these algorithms when applied to periodic orbits.

The paper is organized as follows. ~~Sect. 2 describes briefly~~ Section 2 briefly describes the nonlinear dynamics motivation for undertaking this project, and reviews two existing algorithms related to our work. Readers interested only in the algorithms ~~itself~~ themselves can skip this part. We describe the computational problem in ~~sect. 3.~~ In sect. 4 section 3. In section 4 we deal with the first stage of periodic eigendecomposition, and then show that both the periodic QR algorithm and simultaneous iteration are capable of achieving ~~periodic Schur decomposition.~~ Sect. 5 PSD. Section 5 introduces power iteration and reordering as two practical methods ~~to obtain for obtaining~~ all eigenvectors. In ~~sect. 6~~ section 6 we compare the computational effort required by different methods, and ~~sect. 7~~ section 7 applies periodic eigendecomposition to the Kuramoto–Sivashinsky equation, an example which illustrates the effectiveness of periodic eigendecomposition.

**2. Dynamics background and existing algorithms.** The study of a dynamical system ~~is~~ involves trying to understand the statistical properties of the system and the geometrical structure of the global attractor. As we will see, periodic orbits play an important role in answering both questions. For dissipative systems, orbits typically land ~~onto~~ on an invariant subset, called the global attractor, after a transient period of evolution, and if the system is chaotic, the attractor is a strange attractor which contains a dense set of periodic orbits. The chaotic deterministic flow on this strange attractor can be visualized as a walk chaperoned by a hierarchy of unstable invariant solutions (equilibria, periodic orbits) embedded in the attractor. An ergodic trajectory shadows one such invariant solution for a while, is expelled along its unstable manifold, settles into the neighborhood of another invariant solution for a while, and repeats this process forever. Together, the infinite set of these unstable invariant solutions forms the skeleton of the strange attractor, and ~~in fact,~~ in fact, spatiotemporal averages, such as deterministic diffusion coefficients, energy dissipation rate, and Lyapunov exponents, ~~etc.~~ can be accurately calculated as a summation taken over contributions from periodic orbits weighted by their stabilities [5, 7]. This is one reason we study the algorithm of computing Floquet spectrum in this paper.

On the other hand, recent research on covariant Lyapunov vectors provides numerical evidence [14, 27, 37] that the physical dimension of the inertial manifold [28, 29] of a dissipative PDE can be characterized by a finite number of ~~“entangled”~~ “entangled” modes, dynamically isolated

from the residual set of “isolated” modes. Motivated by the above studies, we anticipate that Floquet vectors display similar properties and can also be used to assess the dimension of the inertial manifold. This is the second reason that we try to formulate a periodic eigendecomposition algorithm suited to accurate computation of Floquet vectors of unstable periodic orbits. Moreover, these studies are based on numerical simulations of long ergodic trajectories, and they yield no intuition about the geometry of the attractor. That is attained by studying the hierarchies of unstable periodic orbits, invariant solutions which, together with their Floquet vectors, provide an effective description of both the local hyperbolicity and the global geometry of an attractor embedded in a high-dimensional state space.

**2.1. Linear stability.** Now, we turn to the definition of Floquet exponents and Floquet vectors. Let the flow of an autonomous continuous system be described by  $\dot{x} = v(x)$ ,  $x \in \mathbb{R}^n$  and the corresponding time-forward trajectory starting from  $x_0$  is  $x(t) = f^t(x_0)$ . In the linear approximation, the deformation of an infinitesimal neighborhood of  $x(t)$  (dynamics in tangent space) is governed by the Jacobian matrix (fundamental matrix)  $\delta x(x, t) = J^t(x_0) \delta x(x_0, t_0)$ , where  $J^t(x_0) = J^{t-t_0}(x_0, t_0) = \partial f^t(x_0) / \partial x_0$ . Jacobian matrix satisfies the semi-group semigroup multiplicative property (chain rule) along an orbit,

$$(2.1) \quad J^{t-t_0}(x(t_0), t_0) = J^{t-t_1}(x(t_1), t_1) J^{t_1-t_0}(x(t_0), t_0).$$

For a periodic point  $x$  on orbit  $p$  of period  $T_p$ ,  $J_p = J^{T_p}(x)$  is called the Floquet matrix (monodromy matrix) and its eigenvalues the Floquet multipliers  $\Lambda_j$ . The  $j$ th Floquet multiplier is a dimensionless ratio of the final/initial perturbation along the  $j$ th eigendirection. It is an intrinsic, local property of a smooth flow, invariant under all smooth coordinate transformations. The associated Floquet vectors  $\mathbf{e}_j(x)$ ,  $J_p \mathbf{e}_j = \Lambda_j \mathbf{e}_j$ , define the invariant directions of the tangent space at periodic point  $x = x(t) \in p$ . Evolving a small initial perturbation aligned with an expanding Floquet direction will generate the corresponding unstable manifold along the periodic orbit. Written in exponential form  $\Lambda_j = \exp(T_p \lambda_p^{(j)}) = \exp(T_p \mu_j + i\theta_j)$ ,  $\Lambda_j = \exp(T_p \lambda_p^{(j)}) = \exp(T_p \mu_j + i\theta_j)$ , with  $\lambda_p^{(j)}$ <sup>1</sup> the Floquet exponents. Floquet multipliers are either real,  $\theta_j = 0, \pi$ , or form complex pairs, i.e.,  $\{\Lambda_j, \Lambda_{j+1}\} = \{|\Lambda_j| \exp(i\theta_j), |\Lambda_j| \exp(-i\theta_j)\}$ ,  $0 < \theta_j < \pi$ . The real parts of Floquet exponents  $\mu_j = (\ln |\Lambda_j|) / T_p$  describe the mean contraction or expansion rates per one period of the orbit. The Jacobian matrix is naively obtained numerically by integrating the stability matrix

$$(2.2) \quad \frac{dJ^t}{dt} = A(x) J^t, \quad \text{with} \quad A(x) = \frac{\partial v(x)}{\partial x}$$

along the orbit. However, it is almost certain that this process will overflow or underflow at an exponential rate as the system evolves, or the resulting Jacobian is highly ill-conditioned. Thus, accurate calculation of expansion rate is not trivial for nonlinear systems, especially for those that evolve in a high-dimensional space. In such cases, the expansion/contraction rates can easily range over many orders of magnitude, which raises poses a challenge to formulating an effective algorithm to tackle this problem. However,

<sup>1</sup>Here, subscript  $p$  emphasizes that it is associated with a periodic orbit so as to distinguish it with Lyapunov exponents defined in the next section.

the ~~semi-group~~ semigroup property (2.1) enables us to factorize the Jacobian matrix into a product of short-time matrices with matrix elements of comparable orders of magnitude. So the problem is reduced to calculating the eigenvalues of the product of a sequence of matrices.

**2.2. Covariant Lyapunov vectors.** *Multiplicative ergodic theorem* [25, 26] says that the forward and backward Oseledets matrices

$$(2.3) \quad \Lambda^\pm(x) := \lim_{t \rightarrow \pm\infty} [J^t(x)^\top J^t(x)]^{1/2t}$$

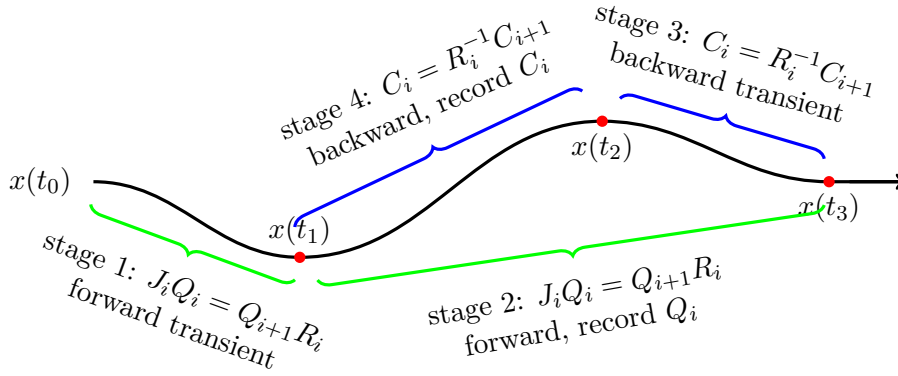
both exist for an invertible dynamical system equipped with an invariant measure. Their eigenvalues are  $e^{\lambda_1^+(x)} < \dots < e^{\lambda_s^+(x)}$  and  $e^{\lambda_1^-(x)} > \dots > e^{\lambda_s^-(x)}$ , respectively, with  $\lambda_i^\pm(x)$  the Lyapunov exponents (characteristic exponents) and  $s$  the total number of distinct exponents ( $s \leq n$ ). For an ergodic system, Lyapunov exponents are the same almost everywhere, and  $\lambda_i^+(x) = -\lambda_i^-(x) = \lambda_i$ . The corresponding eigenspaces  $U_1^\pm(x), \dots, U_s^\pm(x)$  can be used to construct the forward and backward invariant subspaces:  $V_i^+(x) = U_1^+(x) \oplus \dots \oplus U_i^+(x)$ ,  $V_i^-(x) = U_i^-(x) \oplus \dots \oplus U_s^-$ . So the intersections  $W_i(x) = V_i^+(x) \cap V_i^-(x)$  are dynamically forward and backward invariant:  $J^{\pm t}(x)W_i(x) \rightarrow W_i(f^{\pm t}(x))$ ,  $i = 1, 2, \dots, s$ . The expansion rate in invariant subspace  $W_i(x)$  is given by the corresponding Lyapunov exponents,

$$(2.4) \quad \lim_{t \rightarrow \pm\infty} \frac{1}{|t|} \ln \|J^t(x)u\| = \lim_{t \rightarrow \pm\infty} \frac{1}{|t|} \ln \|[J^t(x)^\top J^t(x)]^{1/2}u\| = \pm\lambda_i, \quad u \in W_i(x).$$

If a Lyapunov exponent has degeneracy one, the corresponding subspace  $W_i(x)$  reduces to a vector, called a covariant Lyapunov vector. For periodic orbits, these  $\lambda_i$  (evaluated numerically as  $t \rightarrow \infty$ ) of many repeats of the prime period  $T$ ) coincide with the real part of Floquet exponents (computed in one period of the orbit). Subspace  $W_i(x)$  coincides with a Floquet vector, or, if there is degeneracy, a subspace spanned by Floquet vectors.

The reorthonormalization procedure formulated by Benettin et al. [2] is the standard way to calculate the full spectrum of Lyapunov exponents, and it is shown [9] that the orthogonal vectors produced at the end of ~~calculation converges~~ the calculation converge to  $U_i^-$ , eigenvectors of  $\Lambda^-(x)$  called the ~~Gram-Schmidt~~ Gram-Schmidt (GS) vectors (or backward Lyapunov vectors). Based on this technique, Wolf ~~et al.~~ and Samelson [34] and Ginelli et al. [13, 14] invented independent methods to recover covariant Lyapunov vectors from GS vectors. Here, we should emphasize that GS vectors are not invariant. Except for the leading one, all of them are dependent on the specific inner product imposed by the dynamics. Also, the local expansion rates of covariant Lyapunov vectors are not identical to the local expansion ~~rate~~ es of GS vectors. Specifically for periodic orbits, Floquet vectors depend on no norm, and map forward and backward as  $\mathbf{e}_j \rightarrow J\mathbf{e}_j$  under time evolution. In contrast, the linearized hamics does not transport GS vectors into the tangent space computed further downstream. For a detailed comparison, please see [21, 36].

**2.3. Covariant Lyapunov vector algorithm.** Here we briefly introduce the method used by Ginelli et al. [13, 14] to extract covariant Lyapunov vectors from GS vectors. The setup is the same as computing Lyapunov exponents. We follow a long ergodic trajectory, and integrate the linearized dynamics in tangent space (2.2) with periodic orthonormalization, shown as the



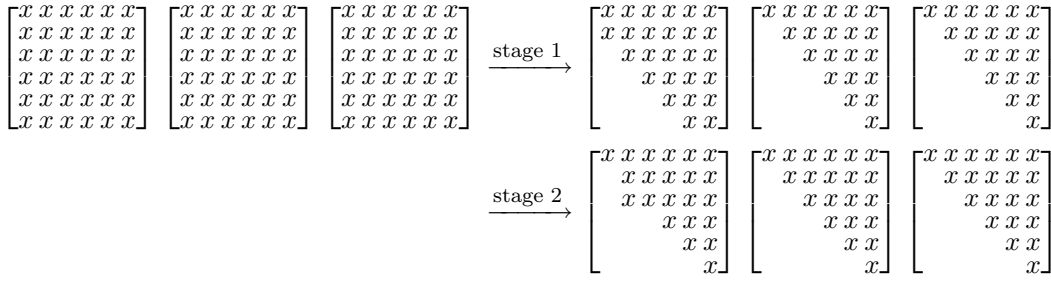
**Figure 1.** Four stages of covariant Lyapunov vector algorithm. The black line is a part of a long ergodic trajectory.

first two stages in Figure 1. Here,  $J_i$  is the short-time Jacobian matrix, and diagonal elements of upper-triangular matrices  $R_i$  store local Lyapunov exponents, ~~long-time~~ the long-time average of which gives the Lyapunov exponents of this system. We assume  $Q_i$  converges to the GS vectors after stage 1, and ~~we~~ start to record  $R_i$  in stage 2. Since the first  $m$  GS vectors span the same subspace as the first  $m$  covariant Lyapunov vectors, ~~which~~ QD means  $W_i = Q_i C_i$ <sup>2</sup> with  $C_i$  an upper-triangular matrix, giving the expansion coefficients of covariant Lyapunov vectors in the GS basis. So we have  $W_i = J_{i-1} Q_{i-1} R_{i-1}^{-1} C_i = J_{i-1} W_{i-1} C_{i-1}^{-1} R_{i-1}^{-1} C_i$ . Since  $W_i$  is invariant in the tangent space, QD ~~hence~~,  $J_{i-1} W_{i-1} = W_i D_i$  with  $D_i$  a diagonal matrix concerning the normalization of covariant Lyapunov vectors. We then obtain the backward dynamics of matrix  $C_i$ :  $C_{i-1} = R_i^{-1} C_i D_i$ . Numerically,  $D_i$  is not formed explicitly since it is only a normalization factor. Ginelli et al. [13, 14] cleverly uncover this backward dynamics and show that  $C_i$  converges after a sufficient number of iterations (stage 3 in Figure 1). This process is continued in stage 4 in Figure 1, and  $C_i$  are recorded at this stage. Finally, we obtain the covariant Lyapunov vectors for trajectory  $x(t_1)$  to  $x(t_2)$  in Figure 1.

~~The Covariant Lyapunov vector~~ covariant Lyapunov vector algorithm is invented to stratify the tangent spaces along an ergodic trajectory, so it is hard to observe degeneracy numerically. However, for periodic orbits, it is possible that some Floquet vectors form conjugate complex pairs. When this algorithm is applied to periodic orbits, it is reduced to a combination of simultaneous iteration and inverse power iteration; consequently, complex conjugate pairs cannot be told apart. This means that we need to pay attention to the ~~two-dimensional~~ two-dimensional rotation when checking the convergence of each stage in Figure 1. As is shown in ~~latter-later~~ sections, a complex conjugate pair of Floquet vectors can be extracted from a converged ~~two-dimensional~~ two-dimensional subspace.

**2.4. Periodic Schur decomposition algorithm.** The double-implicit-shift QR algorithm [31, 33] is the standard way of solving the ~~eigen-problem~~ eigenproblem of a single matrix in

<sup>2</sup>Here,  $W_i$  refers to the matrix whose columns are covariant Lyapunov vectors at step  $i$  of the algorithm. Do not get confused with the ~~i-th~~ i-th covariant Lyapunov vector.



**Figure 2.** Two stages of ~~periodic Schur decomposition~~the PSD algorithm illustrated by three  $[6 \times 6]$  matrices. Empty locations are zeros.

many numerical packages, such as the `eig()` function in [Matlab](#). [Bojanczyk et al.](#) [MATLAB](#). [Bojanczyk, Golub, and Van Dooren](#) [3] ~~extend~~ extended this idea to obtain ~~periodic Schur decomposition~~PSD of the product of a sequence of matrices. Later on, [Kurt-Lust](#) [23] ~~describes~~ described the implementation details and ~~provides~~ provided the corresponding Fortran code. As stated before, by use of [the](#) chain rule (2.1), [a](#) Jacobian matrix can be decomposed into a product of short-time Jacobians with the same dimension, so ~~periodic Schur decomposition~~PSD is suitable for computing Floquet exponents, and we think it is necessary to introduce this algorithm to the physics community.

As illustrated in ~~periodic Schur decomposition~~Figure 2, PSD proceeds in two stages. First, the sequence of matrices is transformed to ~~Hessenberg-Triangular~~[Hessenberg-triangular](#) form, ~~one of which~~ [were one matrix](#) has upper-Hessenberg form, while the others are upper-triangular, by a series of Householder transformations [31]. The second stage tries to diminish the ~~sub-diagonal~~subdiagonal components of the Hessenberg matrix until it becomes quasi-upper-triangular, that is, there are some  $[2 \times 2]$  blocks on the diagonal corresponding to complex eigenvalues. Then the eigenvalues of the matrix product are given by the products of all individual matrices' diagonal elements. However, ~~periodic Schur decomposition~~PSD is not enough for extracting eigenvectors except the leading one. [Kurt-Lust](#) [23] claims to formulate the corresponding Floquet vector algorithm, but to the best of our knowledge, such [an](#) algorithm is not present in [the](#) literature. Fortunately, [Granat and Ket-ålgström](#) [16] propose a method to reorder diagonal elements after ~~periodic Schur decomposition~~PSD. It provides an elegant way to compute Floquet vectors, as we will see in later sections.

**3. Description of the problem.** After introducing the underlying physical motivation, let us turn to the definition of the problem. According to (2.1), Jacobian matrix can be integrated piece by piece along a state orbit:


$$J^t(x_0) = J^{t_m-t_{m-1}}(x(t_{m-1}), t_{m-1}) \cdots J^{t_2-t_1}(x(t_1), t_1) J^{t_1-t_0}(x(t_0), t_0)$$

with  $t_0 = 0$ ,  $t_m = t$ , and  $x_0$  the initial point. For periodic orbits,  $x(t_m) = x_0$ . The time sequence  $t_i$ ,  $i = 1, 2, \dots, m-1$   ~~$i = 1, 2, \dots, m-1$~~  is chosen properly such that the elements of Jacobian matrix associated with each small time interval have relatively similar ~~order~~orders




of magnitude. For simplicity, we drop all the parameters above and use a bold letter to denote the product:

$$(3.1) \quad \mathbf{J}^{(0)} = J_m J_{m-1} \cdots J_1, \quad J_i \in \mathbb{R}^{n \times n}, \quad i = 1, 2, \dots, m.$$

This product can be diagonalized if and only if the sum of dimensions of eigenspaces of  $\mathbf{J}^{(0)}$  is  $n$ . 

$$(3.2) \quad \mathbf{J}^{(0)} = E^{(0)} \Sigma (E^{(0)})^{-1},$$



where  $\Sigma$  is a diagonal matrix which stores  $\mathbf{J}^{(0)}$ 's eigenvalues (Floquet multipliers),  $\{\Lambda_1, \Lambda_2, \dots, \Lambda_n\}$ , and columns of matrix  $E^{(0)}$  are the eigenvectors (Floquet vectors) of  $\mathbf{J}^{(0)}$ :  $E^{(0)} = [\mathbf{e}_1^{(0)}, \mathbf{e}_2^{(0)}, \dots, \mathbf{e}_n^{(0)}]$ . In this paper all vectors are written in the column form, the transpose of  $v$  is denoted  $v^\top$ , and Euclidean 'dot' product the Euclidean "dot" product is denoted by  $(v^\top u)$ . The challenge associated with obtaining diagonalized form (3.2) is the fact that often  $\mathbf{J}^{(0)}$  should not be written explicitly since the integration process (2.2) may overflow or the resulting matrix  highly ill-conditioned. Floquet multipliers can easily vary over hundreds of orders of magnitude, depending on the system under study and the period of the orbit; therefore, all transformations should be applied to the short-time Jacobian matrices  $J_i$  individually, instead of working with the full-time  $\mathbf{J}^{(0)}$ . Also, in order to characterize the geometry along a periodic orbit, not only are the Floquet vectors at the initial point are required, but also the sets at each point on the orbit. Therefore, we also desire the eigendecomposition of the cyclic rotations of  $\mathbf{J}^{(0)}$ :  $\mathbf{J}^{(k)} = J_k J_{k-1} \cdots J_1 J_m \cdots J_{k+1}$  for  $k = 1, 2, \dots, m-1$ . Eigendecomposition of all  $\mathbf{J}^{(k)}$  is called the *periodic eigendecomposition* of the matrix sequence  $J_m, J_{m-1}, \dots, J_1, J_m, J_{m-1}, \dots, J_1$ .

The process of implementing eigendecomposition (3.2) proceeds in two stages. First, periodic real Schur form (PRSF) is obtained by a similarity transformation for each  $J_i$ ,

$$(3.3) \quad J_i = Q_i R_i Q_i^\top,$$

with  $Q_i$  orthogonal matrix and  $Q_0 = Q_m$ . One of  $R_i$  above is quasi-upper-triangular quasi-upper-triangular with  $[1 \times 1]$  and  $[2 \times 2]$  blocks on the diagonal, and the others are all upper-triangular upper-triangular. Since the definition of  $\mathbf{J}^{(k)}$  is cyclic, we can choose  $R_m$  to be quasi-upper-triangular quasi-upper-triangular without loss of generality. The existence of PRSF, proved in [3], provides the periodic QR algorithm that implements periodic Schur decomposition PSD. Defining  $\mathbf{R}^{(k)} = R_k R_{k-1} \cdots R_1 R_m \cdots R_{k+1}$ , we have

$$(3.4) \quad \mathbf{J}^{(k)} = Q_k \mathbf{R}^{(k)} Q_k^\top,$$

with the eigenvectors of matrix  $\mathbf{J}^{(k)}$  related to eigenvectors of quasi-upper-triangular quasi-upper-triangular matrix  $\mathbf{R}^{(k)}$  by orthogonal matrix  $Q_k$ .  $\mathbf{J}^{(k)}$  and  $\mathbf{R}^{(k)}$  have the same eigenvalues, stored in the  $[1 \times 1]$  and  $[2 \times 2]$  blocks on the diagonal of  $\mathbf{R}^{(k)}$ , and their eigenvectors are transformed by  $Q_k$ , so the second stage concerns the eigendecomposition of  $\mathbf{R}^{(k)}$ . Eigenvector-The eigenvector matrix of  $\mathbf{R}^{(k)}$  has the same structure as  $R_m$ . We evaluate it by two distinct algorithms. The first one is power iteration, while the second algorithm relies on solving a periodic Sylvester equation [16].

As all  $\mathbf{R}^{(k)}$  have the same eigenvalues, and their eigenvectors are related by similarity transformations,

$$(3.5) \quad \mathbf{R}^{(k)} = (R_m \cdots R_{k+1})^{-1} \mathbf{R}^{(0)} (R_m \cdots R_{k+1}),$$

one may be tempted to calculate the eigenvectors of  $\mathbf{R}^{(0)}$  and obtain the eigenvectors of  $\mathbf{R}^{(k)}$  by (3.5). The pitfall of this approach is that numerical errors accumulate when multiplying a sequence of upper triangular matrices, especially for large  $k$ , such that contracting eigenvectors are contaminated by expanding ones during this process.

Our work illustrates the connection between different algorithms in the two stages of implementing periodic eigendecomposition, pays attention to the case when eigenvectors appear as complex pairs, and demonstrates that eigenvectors can be obtained directly from a periodic Sylvester equation without restoring PRSF.


**4. Stage 1: Periodic real Schur form.** This is the first stage of implementing periodic eigendecomposition. Equation (3.4) represents the eigenvalues of matrix  $\mathbf{J}^{(k)}$  as real eigenvalues on the diagonal, and complex eigenvalue pairs as  $[2 \times 2]$  blocks on the diagonal of  $\mathbf{R}^{(k)}$ . More specifically, if the  $i$ th eigenvalue is real, it is given by the product of all the  $i$ th diagonal elements of matrices  $R_1, R_2, \dots, R_m$ . In practice, the logarithms of magnitudes of these numbers are added in order to overcome numerical overflow or underflow. If the  $i$ th and  $(i+1)$ th eigenvalues form a complex conjugate pair, all  $[2 \times 2]$  matrices at position  $(i, i+1)$  on the diagonal of  $R_1, R_2, \dots, R_m$  are multiplied with normalization at each step, and the two complex eigenvalues of the product are obtained. There is no danger of numerical overflow or underflow because all of these  $[2 \times 2]$  matrices are in the same position, and in our applications their elements are of similar order of magnitude. Section 2.4 introduces the periodic Schur decomposition PSD to achieve PRSF. An alternative is the first two stages of the covariant Lyapunov vector algorithm in section 2.3, which reduces to simultaneous iteration for periodic orbits. Actually, for a single matrix, simultaneous iteration is equivalent to iteration [31]. When it comes to the matrix product, simultaneous iteration and periodic Schur decomposition PSD both achieve the PRSF, but their computational complexities differ.

**Simultaneous iteration.** The basic idea of simultaneous iteration is implementing QR decomposition in the process of power iteration. Assume all Floquet multipliers are real, without degeneracy, and order them by their magnitude:  $|\Lambda_1| > |\Lambda_2| > \cdots > |\Lambda_n|$ , with corresponding normalized Floquet vectors  $\mathbf{e}_1, \mathbf{e}_2, \dots, \mathbf{e}_n$ . For simplicity, here we have dropped the upper indices of these vectors. An arbitrary initial vector  $\tilde{q}_1 = \sum_{i=1}^n \alpha_i^{(1)} \mathbf{e}_i$  will converge to the first Floquet vector  $\mathbf{e}_1$  after normalization under power iteration of  $\mathbf{J}^{(0)}$ ,

$$\lim_{\ell \rightarrow \infty} \frac{(\mathbf{J}^{(0)})^\ell \tilde{q}_1}{\|\cdot\|} \rightarrow q_1 = \mathbf{e}_1.$$

Here  $\|\cdot\|$  denotes the Euclidean norm of the numerator ( $\|x\| = \sqrt{x^\top x}$ ). Let  $\langle \mathbf{a}, \mathbf{b}, \dots, \mathbf{e} \rangle$  represent the space spanned by vector  $\mathbf{a}, \mathbf{b}, \dots, \mathbf{e}$  in  $\mathbb{R}^n$ . Another arbitrary vector  $\tilde{q}_2$  is then chosen orthogonal to subspace  $\langle q_1 \rangle$  by Gram-Schmidt-GM orthonormalization,  $\tilde{q}_2 = \sum_{i=2}^n \alpha_i^{(2)} [\mathbf{e}_i - (q_1^\top \mathbf{e}_i) q_1]$ . Note that the index starts from  $i = 2$  because



$\langle q_1 \rangle = \langle \mathbf{e}_1 \rangle$ . The strategy now is to apply power iteration of  $\mathbf{J}^{(0)}$  followed by orthonormalization in each iteration. 


$$\mathbf{J}^{(0)} \tilde{q}_2 = \sum_{i=2}^n \alpha_i^{(2)} [\Lambda_i \mathbf{e}_i - \Lambda_1 (q_1^\top \mathbf{e}_i) q_1] = \sum_{i=2}^n \alpha_i^{(2)} \Lambda_i [\mathbf{e}_i - (q_1^\top \mathbf{e}_i) q_1] + \sum_{i=2}^n \alpha_i^{(2)} (\Lambda_i - \Lambda_1) (q_1^\top \mathbf{e}_i) q_1.$$

The second term in the above expression will disappear after performing ~~Gram-Schmidt~~ GM orthonormalization to  $\langle q_1 \rangle$ , and the first term will converge to  $q_2 = \mathbf{e}_2 - (q_1^\top \mathbf{e}_2) q_1$  (not normalized) after a sufficient number of iterations because of the descending magnitudes of  $\Lambda_i$ , and we also note that  $\langle \mathbf{e}_1, \mathbf{e}_2 \rangle = \langle q_1, q_2 \rangle$ . The same argument can be applied to  ~~$\tilde{q}_i, i = 3, 4, \dots, n$~~   $\tilde{q}_i, i = 3, 4, \dots, n$ , as well. In this way, after a sufficient number of iterations,

$$\lim_{\ell \rightarrow \infty} (\mathbf{J}^{(0)})^\ell [\tilde{q}_1, \tilde{q}_2, \dots, \tilde{q}_n]^\ell [\tilde{q}_1, \tilde{q}_2, \dots, \tilde{q}_n] \rightarrow [q_1, q_2, \dots, q_n],$$

where

$$q_1 = \mathbf{e}_1, \quad q_2 = \frac{\mathbf{e}_2 - (\mathbf{e}_2^\top q_1) q_1}{\|\cdot\|}, \quad \dots, \quad q_n = \frac{\mathbf{e}_n - \sum_{i=1}^{n-1} (\mathbf{e}_n^\top q_i) q_i}{\|\cdot\|}.$$

Let matrix  ~~$Q_0 = [q_1, q_2, \dots, q_n]$~~   $Q_0 = [q_1, q_2, \dots, q_n]$ ; then we have  $\mathbf{J}^{(0)} Q_0 = Q_0 \mathbf{R}^{(0)}$  with  $\mathbf{R}^{(0)}$  an ~~upper triangular~~ upper-triangular matrix because of  $\langle q_1, q_2, \dots, q_i \rangle = \langle \mathbf{e}_1, \mathbf{e}_2, \dots, \mathbf{e}_i \rangle \langle q_1, q_2, \dots, q_i \rangle = \langle \mathbf{e}_1, \mathbf{e}_2, \dots, \mathbf{e}_i \rangle$  which is just  $\mathbf{J}^{(0)} = Q_0 \mathbf{R}^{(0)} Q_0^\top$  (the Schur decomposition of  $\mathbf{J}^{(0)}$ ). The diagonal elements of  $\mathbf{R}^{(0)}$  are the eigenvalues of  $\mathbf{J}^{(0)}$  in decreasing order. Numerically, the process described above can be implemented on an arbitrary initial full rank matrix  $\tilde{Q}_0$  followed by QR decomposition at each step. 

$$(4.1) \quad J_s \tilde{Q}_{s-1} = \tilde{Q}_s \tilde{R}_s$$

with  ~~$s = 1, 2, 3, \dots$~~   $s = 1, 2, 3, \dots$  and  $J_{s+m} = J_s$ . For a sufficient number of iterations,  $\tilde{Q}_s$  and  $\tilde{R}_s$  converge to  $Q_s$  and  $R_s$  in (3.3) for  ~~$s = 1, 2, \dots, m$~~   $s = 1, 2, \dots, m$ , so we achieve (3.4) the ~~periodic Schur decomposition~~ PSD of  $\mathbf{J}^{(k)}$ .

We have thus demonstrated that simultaneous iteration converges to PRSF for real non-degenerate eigenvalues. For complex eigenvalue pairs, the algorithm converges in the sense that the subspace spanned by a complex conjugate vector pair converges. So,

$$(4.2) \quad \mathbf{J}^{(0)} Q_0 = Q'_0 \mathbf{R}^{(0)} = Q_0 D \mathbf{R}^{(0)},$$

where  $D$  is a block-diagonal matrix with diagonal elements  $\pm 1$  (corresponding to real eigenvalues) or  $[2 \times 2]$  blocks (corresponding to complex eigenvalue pairs). Absorb  $D$  into  $R_m$ ; then  $R_m$  becomes a ~~quasi-upper triangular~~ quasi-upper-triangular matrix, and (3.3) still holds. Here, we focus on  $Q_0$  instead of  ~~$Q_1, \dots, Q_{m-1}$~~   $Q_1, \dots, Q_{m-1}$  because we assume  $R_m$  is ~~quasi-upper triangular~~ quasi-upper-triangular in (3.3).

**5. Stage 2: Eigenvector algorithms.** Upon achieving PRSF, the eigenvectors of  $\mathbf{J}^{(k)}$  are related to the eigenvectors of  $\mathbf{R}^{(k)}$  by orthogonal matrix  $Q_k$  from (3.3), and the eigenvector matrix of  $\mathbf{R}^{(k)}$  has the same ~~quasi-upper-triangular~~ quasi-upper-triangular structure as  $R_m$ . In addition, if we follow the simultaneous iteration method or implement ~~periodic Schur decomposition~~ PSD without shift, eigenvalues are ordered by their magnitudes on the diagonal. Power iteration utilizing this property could be easily implemented to generate the eigenvector matrix. This is the basic idea of the first algorithm for generating eigenvectors of  $\mathbf{R}^{(k)}$ , corresponding to the ~~3rd and 4th stage in~~ third and fourth stages in the covariant Lyapunov vector algorithm in Figure 1. Alternatively, ~~observation~~ observing that the first eigenvector of  $\mathbf{R}^{(k)}$  is trivial if it is real,  $v_1 = (1, 0, \dots, 0)^\top$ ,  $v_1 = (1, 0, \dots, 0)^\top$ , inspires us to reorder the eigenvalues so that the  ~~$j$ th~~  $j$ th eigenvalue is in the first diagonal place of  $\mathbf{R}^{(k)}$ ; in this way, the  ~~$j$ th~~  $j$ th eigenvector is obtained. For both methods, attention should be paid to the complex conjugate eigenvector pairs. In this section,  $v_i^{(k)}$  denotes the  ~~$i$ th~~  $i$ th eigenvector of  $\mathbf{R}^{(k)}$ , contrast to  $e_i^{(k)}$  the eigenvectors of  $\mathbf{J}^{(k)}$ , and for most cases, the upper indices are dropped if no confusion occurs.

**5.1. Iteration method.** The prerequisite for the iteration method is that all the eigenvalues are ordered in an ascending or descending way by their ~~magnitude~~ magnitudes on the diagonal of  $\mathbf{R}^{(k)}$ . Assume that they are in descending order, which is the outcome of simultaneous iteration; therefore, the diagonal elements of  $\mathbf{R}^{(k)}$  are  ~~$\Lambda_1, \Lambda_2, \dots, \Lambda_n$~~   $\Lambda_1, \Lambda_2, \dots, \Lambda_n$ , with magnitudes from large to small. If the  ~~$i$ th~~  $i$ th eigenvector of  $\mathbf{R}^{(k)}$  is real, then it has form  $v_i = (a_1, a_2, \dots, a_i, 0, \dots, 0)^\top$ ,  $v_i = (a_1, a_2, \dots, a_i, 0, \dots, 0)^\top$ . An arbitrary vector whose first  $i$  elements are nonzero  $x = (b_1, b_2, \dots, b_i, 0, \dots, 0)^\top$  is a linear combination of the first  $i$  eigenvectors:  $x = \sum_{j=1}^i \alpha_j v_j$ . Use it as the initial condition for the power iteration by  $(\mathbf{R}^{(k)})^{-1} = R_{k+1}^{-1} \dots R_m^{-1} R_1^{-1} R_2^{-1} \dots R_k^{-1}$ , and after a sufficient number of iterations,

$$(5.1) \quad \lim_{\ell \rightarrow \infty} \frac{(\mathbf{R}^{(k)})^{-\ell} x}{\|\cdot\|} = v_i.$$

The property we used here is that  $(\mathbf{R}^{(k)})^{-1}$  and  $\mathbf{R}^{(k)}$  have the same eigenvectors but inverse eigenvalues. Moreover, matrix sequence  $R_{k+1}^{-1} \dots R_m^{-1} R_1^{-1} R_2^{-1} \dots R_k^{-1}$  is applied sequentially in (5.1), so if the  ~~$i$ th~~  $i$ th eigenvector  $v_i^{(k)}$  of  $(\mathbf{R}^{(k)})^{-1}$  converges, then the  ~~$i$ th~~  $i$ th eigenvector of  $(\mathbf{R}^{(k-1)})^{-1}$  is obtained by  $v_i^{(k-1)} = R_k^{-1} v_i^{(k)}$  and to be normalized). Therefore, the  ~~$i$ th~~  $i$ th eigenvectors of  $(\mathbf{R}^{(k)})$  for  ~~$k = 0, 1, \dots, m$~~   $k = 0, 1, \dots, m$  are obtained almost simultaneously. Note that there is no numerical instability here as in (3.5) because (5.1) finds the most expanding direction in the subspace that only the first  $i$  elements are nonzero.

For a  ~~$[2 \times 2]$~~   $[2 \times 2]$  block on the diagonal of  $\mathbf{R}^{(k)}$ , the corresponding conjugate complex eigenvectors form a ~~two-dimensional~~ two-dimensional subspace. Any real vector selected from this subspace will rotate under power iteration. In this case, power iteration still converges in the sense that the subspace spanned by the complex conjugate eigenvector pair converges. Suppose the  ~~$i$ th and  $(i+1)$ th~~  $i$ th and  $(i+1)$ th eigenvectors of  $\mathbf{R}^{(k)}$  form a complex pair. Two arbitrary vectors  $x_1$  and  $x_2$  whose first  $i+1$  elements are ~~non-zero~~ nonzero can be written as the linear superposition of the first  $i+1$  eigenvectors,  $x_{1,2} = (\sum_{j=1}^{i-1} \alpha_j^{(1,2)} v_j) + \alpha_i^{(1,2)} v_i + (\alpha_i^{(1,2)} v_i)^*$ , where  $(*)$  denotes the complex conjugate. As for the real case, the first  $i-1$  components will

vanish after a sufficient number of iterations. Denote the two vectors at this instance to be  $X_{1,2}$ , and form matrix  $X = [X_1, X_2]$ . The subspace spanned by  $X_{1,2}$  does not change, and  $X$  will be rotated after another iteration,

$$(5.2) \quad (\mathbf{R}^{(k)})^{-1}X = X' = XC,$$

where  $C$  is a  $[2 \times 2]$  matrix which has two complex conjugate eigenvectors  $v_C$  and  $(v_C)^*$ . Transformation (5.2) relates the eigenvectors of  $\mathbf{R}^{(k)}$  with those of  $C$ :  $[v_i, (v_i)^*] = X[v_C, (v_C)^*]$ . In practice, matrix  $C$  can be computed by QR decomposition; if we let  $X = Q_X R_X$  be the QR decomposition of  $X$ , then  $C = R_X^{-1} Q_X^\top X'$ . On the other hand, complex eigenvectors are not uniquely determined in the sense that  $e^{i\theta} v_i$  is also an eigenvector with the same eigenvalue as  $v_i$  for an arbitrary phase  $\theta$ , so when comparing results from different eigenvector algorithms, we need a constraint to fix the phase of a complex eigenvector, such as letting the first element be real.

We should note that performance of power iteration depends on the ratios of magnitudes of eigenvalues, so performance is poor for systems with clustered eigenvalues. We anticipate that proper modifications, such as shifted iteration or inverse iteration [31], may help improve the performance. Such techniques are beyond the scope of this paper.

**5.2. Reordering method.** There exists a direct algorithm to obtain the eigenvectors of every  $\mathbf{R}^{(k)}$  at once without iteration. The idea is very simple: the eigenvector corresponding to the first diagonal element of an upper-triangular matrix is  $v_1 = (1, 0, \dots, 0)^\top$ . By reordering the diagonal elements (or  $[2 \times 2]$  blocks) of  $\mathbf{R}^{(0)}$ , we can find any eigenvector by positioning the corresponding eigenvalue in the first diagonal position. Although in our application only reordering of  $[1 \times 1]$  and  $[2 \times 2]$  blocks is needed, we recapitulate here the general case of reordering two adjacent blocks of a quasi-upper-triangular matrix following Granat et al. and Kågström [16]. Partition  $R_i$  as

$$R_i = \left[ \begin{array}{c|c|c|c} R_i^{00} & * & * & * \\ \hline 0 & R_i^{11} & R_i^{12} & * \\ \hline 0 & 0 & R_i^{22} & * \\ \hline 0 & 0 & 0 & R_i^{33} \end{array} \right],$$

where  $R_i^{00}, R_i^{11}, R_i^{22}, R_i^{33}$  have size  $[p_0 \times p_0], [p_1 \times p_1], [p_2 \times p_2]$  and  $[p_3 \times p_3]$ , respectively, and  $p_0 + p_1 + p_2 + p_3 = n$ . In order to exchange the middle two blocks ( $R_i^{11}$  and  $R_i^{22}$ ), we construct a nonsingular periodic matrix sequence  $\hat{S}_i, i = 0, 1, 2, \dots, m$ , with  $\hat{S}_0 = \hat{S}_m$ , as

$$\hat{S}_i = \left[ \begin{array}{c|c|c} I_{p_0} & 0 & 0 \\ \hline 0 & S_i & 0 \\ \hline 0 & 0 & I_{p_3} \end{array} \right],$$

where  $S_i$  is a  $[(p_1 + p_2) \times (p_1 + p_2)]$  matrix, such that  $\hat{S}_i$  transforms  $R_i$  as follows:

$$(5.3) \quad \hat{S}_i^{-1} R_i \hat{S}_{i-1} = \tilde{R}_i = \left[ \begin{array}{c|c|c|c} R_i^{00} & * & * & * \\ \hline 0 & R_i^{22} & 0 & * \\ \hline 0 & 0 & R_i^{11} & * \\ \hline 0 & 0 & 0 & R_i^{33} \end{array} \right],$$

which is

$$S_i^{-1} \begin{bmatrix} R_i^{11} & R_i^{12} \\ 0 & R_i^{22} \end{bmatrix} S_{i-1} = \begin{bmatrix} R_i^{22} & 0 \\ 0 & R_i^{11} \end{bmatrix}.$$

The problem is to find the appropriate matrices  $S_i$  which satisfy the above condition. Assume that  $S_i$  has form

$$S_i = \begin{bmatrix} X_i & I_{p_1} \\ I_{p_2} & 0 \end{bmatrix},$$

where matrix  $X_i$  has dimension  $[p_1 \times p_2]$ . We obtain the periodic Sylvester equation [16]

$$(5.4) \quad R_i^{11} X_{i-1} - X_i R_i^{22} = -R_i^{12}, \quad i = 0, 1, 2, \dots, m.$$

The algorithm to find eigenvectors is based on (5.4). If the  ~~$i_{th}$~~   $i_{th}$  eigenvalue of  $\mathbf{R}^{(k)}$  is real, we ~~only need to~~ need only exchange the leading  $[(i-1) \times (i-1)]$  block of  ~~$R_k, k=1, 2, \dots, m$~~  with its  $i_{th}$   $R_k, k=1, 2, \dots, m$ , with its  $i_{th}$  diagonal element. If the  ~~$i_{th}$  and  $(i+1)_{th}$~~   $i_{th}$  and  $(i+1)_{th}$  eigenvalues form a complex conjugate pair, then the leading  $[(i-1) \times (i-1)]$  block and the following  $[2 \times 2]$  block should be exchanged. Therefore  $X_i$  in (5.4) has dimension  $[p_1 \times 1]$  or  $[p_1 \times 2]$ . In both cases,  $p_0 = 0$ .

Real eigenvectors. In this case, matrix  $X_i$  is just a column vector, so (5.4) is equivalent to

$$(5.5) \quad \begin{bmatrix} R_1^{11} & -R_1^{22} I_{p_1} & & & \\ & R_2^{11} & -R_2^{22} I_{p_1} & & \\ & & R_3^{11} & -R_3^{22} I_{p_1} & \\ & & & \ddots & \dots \\ & & & & R_m^{11} \\ -R_m^{22} I_{p_1} & & & & \end{bmatrix} \begin{bmatrix} X_0 \\ X_1 \\ X_2 \\ \dots \\ X_{m-1} \end{bmatrix} = \begin{bmatrix} -R_1^{12} \\ -R_2^{12} \\ -R_3^{12} \\ \dots \\ -R_m^{12} \end{bmatrix},$$

where  $R_i^{22}$  is the  ~~$(p_1+1)_{th}$~~   $(p_1+1)_{th}$  diagonal element of  $R_i$ . The accuracy of the eigenvectors is determined by the accuracy of solving the sparse linear equation (5.5). In our application to periodic orbits in ~~one-dimensional~~ the one-dimensional Kuramoto–Sivashinsky equation, Gaussian elimination with partial pivoting (GEPP) is enough. For a more technical treatment, such as cyclic reduction or preconditioned conjugate gradients, ~~to name a few,~~ please see [1, 10, 15].

Now we get all vectors  $X_i$  by solving a periodic Sylvester equation, but how are they related to the eigenvectors? In analogy to  $\mathbf{R}^{(0)}$ , defining  $\tilde{\mathbf{R}}_0 = \tilde{R}_m \tilde{R}_{m-1} \cdots \tilde{R}_1$ , we get  $\hat{S}_m^{-1} \mathbf{R}^{(0)} \hat{S}_m = \tilde{\mathbf{R}}_0$  by (5.3). Since  $p_0 = 0$  and  $p_2 = 1$  in (5.3), the first eigenvector of  $\tilde{\mathbf{R}}_0$ , the one corresponding to eigenvalue  $\Lambda_{p_1+1}$  ~~is  $\tilde{e} = (1, 0, \dots, 0)^T$~~  is  $\tilde{e} = (1, 0, \dots, 0)^T$ . Apart from normalization, the corresponding eigenvector of  $\mathbf{R}^{(0)}$  is

$$v_{p_1+1}^{(0)} = \hat{S}_m \tilde{e} = \begin{bmatrix} X_0^T, 1, 0, 0, \dots, 0 \end{bmatrix}^T.$$

This is the eigenvector of matrix  $\mathbf{R}^{(0)} = R_m R_{m-1} \cdots R_1$  in (3.4) for  $k = 0$ . For  $\mathbf{R}^{(1)} = R_1 R_m \cdots R_2$ , the corresponding periodic Sylvester equation will be cyclically rotated one row

up in (5.5), which means  $X_1$  will be shifted to the first place, and thus the corresponding eigenvector of  $\mathbf{R}^{(1)}$  is  $v_{p_1+1}^{(1)} = [X_1^\top, 1, 0, \dots, 0]^\top$ . The same argument goes for all the  $\mathbf{R}^{(k)}$ . In conclusion, the solution of (5.5) contains the eigenvectors for all  $\mathbf{R}^{(k)}, k = 0, 1, \dots, m-1$ . Another benefit of the reordering method is that we can selectively get the eigenvectors corresponding to some specific eigenvalues. This merit is important in high-dimensional nonlinear systems for which only a subset of Floquet vectors suffices to characterize the dynamics in tangent space, and thus we avoid wasting time in calculating the remaining unimportant subset.

**Complex eigenvector pairs.** As in the real eigenvalue case, we have  $p_0 = 0$ , but now  $p_2 = 2$ , so matrix  $X_i$  has dimension  $[p_1 \times 2]$ . Using the same notation as in [16], let  $v(X_i)$  denote the vector representation of  $X_i$  with the columns of  $X_i$  stacked on top of each other, and let  $A \otimes B$  denote the Kronecker product of two matrices, with the  $(i, j)$ -block element  $a_{ij}B$ .

Now, the periodic Sylvester equation (5.4) is equivalent to

$$(5.6) \quad \begin{bmatrix} I_2 \otimes R_1^{11} & -(R_1^{22})^\top \otimes I_{p_1} & & & \\ & I_2 \otimes R_2^{11} & -(R_2^{22})^\top \otimes I_{p_1} & & \\ & & I_2 \otimes R_3^{11} & -(R_3^{22})^\top \otimes I_{p_1} & \\ & & & \ddots & \dots \\ & & & & I_2 \otimes R_m^{11} \\ -(R_m^{22})^\top \otimes I_{p_1} & & & & \end{bmatrix} \begin{bmatrix} v(X_0) \\ v(X_1) \\ v(X_2) \\ \dots \\ v(X_{m-1}) \end{bmatrix} = \begin{bmatrix} -v(R_1^{12}) \\ -v(R_2^{12}) \\ -v(R_3^{12}) \\ \dots \\ -v(R_m^{12}) \end{bmatrix}.$$



After switching  $R_i^{11}$  and  $R_i^{22}$ , we can get the first two eigenvectors of  $\tilde{\mathbf{R}}_0$  by multiplying the first  $[2 \times 2]$  diagonal blocks of  $\tilde{R}_i$ :  $R^{22} = R_m^{22} R_{m-1}^{22} \dots R_1^{22}$ . Let the eigenvectors of  $R^{22}$  be  $v$  and  $v^*$  of size  $[2 \times 1]$ ; then the corresponding eigenvectors of  $\tilde{\mathbf{R}}_0$  are  $\tilde{e}_1 = (v^\top, 0, 0, \dots, 0)^\top$  and  $\tilde{e}_2 = (\tilde{e}_1)^*$  (the additional zeros make the length of the eigenvectors be  $n$ ). Therefore, the corresponding eigenvectors of  $\mathbf{R}^{(0)}$  are


$$\begin{bmatrix} v_{p_1+1}^{(0)} \\ v_{p_1+2}^{(0)} \end{bmatrix} = \hat{S}_m[\tilde{e}_1, \tilde{e}_2] = \begin{bmatrix} X_0 \\ I_2 \\ 0 & 0 \\ 0 & 0 \\ \vdots \\ 0 & 0 \end{bmatrix} [v, v^*].$$

For other  $\mathbf{R}^{(k)}$ , the same argument as in the real case applies here, too, so we obtain all the complex eigenvector pairs for  $\mathbf{R}^{(k)}, k = 1, 2, \dots, m$ .

**6. Computational complexity and convergence analysis.** In this paper we make no attempt at conducting a strict error analysis of the algorithms presented. However, for practical applications, it is important to understand their computational costs. Periodic eigendecomposition is conducted in two stages: (1) PRSF, and (2) determination of all

eigenvectors. In each stage, there are two candidate algorithms, so the efficiency of periodic eigendecomposition depends on the choice of the specific algorithm chosen in each stage.



~~Periodic Schur decomposition~~The PSD algorithm and simultaneous iteration are both effective ~~to achieve in achieving~~ PRSF. We estimate the complexity of ~~periodic Schur decomposition~~the PSD algorithm in analogy with the single matrix case. For a single  $[n \times n]$  matrix,  $O(n^3)$  flops (floating-point operations) are required [31] to reduce it to ~~upper-Hessenberg~~upper-Hessenberg form. Accordingly, the first stage in Figure 2 takes  $O(mn^3)$  flops. Then the implicit  iteration process for a single matrix takes  $O(n^2)$  flops for a single iteration, so each iteration of the second stage in Figure 2 takes  $O(mn^2)$  flops. Usually, the number of iterations ~~exceeds~~ ~~by far far exceeds~~ the dimension of the matrix. Therefore, the average complexity of one iteration in ~~periodic Schur decomposition~~the PSD algorithm is  $O(mn^2)$ . For ~~detailed discussion~~ ~~a detailed discussion~~, see [3, 31]. On the other hand, simultaneous iteration (4.1) requires  $m$  QR  composition  $O(mn^3)$  and  $m$  matrix-matrix ~~multiplication~~  $O(mn^3)$  in each iteration, giving a total computational cost of  $O(mn^3)$ . Moreover, the convergence of both algorithms depends linearly on the ratio of adjacent eigenvalues of  $\mathbf{R}^{(0)}$ :  $|\Lambda_i|/|\Lambda_{i+1}|$  without shift [11]. Therefore, the ratio of costs between ~~periodic Schur decomposition~~the PSD algorithm and simultaneous iteration is approximately of the order  $O(mn^2)/O(mn^3) = O(1/n)$ , implying that the ~~periodic Schur decomposition~~PSD algorithm is much cheaper than the simultaneous iteration if the dimension of matrices involved is large.

The second stage of periodic eigendecomposition is to find all the eigenvectors of  $\mathbf{J}^{(k)}$  via ~~quasi-upper-triangular~~quasi-upper-triangular matrices  $\mathbf{R}^{(k)}$ . The first candidate is power iteration. The computational cost of one iteration (5.1) for the  ~~$i$ th~~ $i$ th eigenvector is  $O(mi^2)$ . The second candidate, ~~the~~reordering method, relies on an effective method to solve ~~the~~periodic Sylvester equation (5.4). For example, GEPP is suitable for ~~the~~well-conditioned ~~matrix~~  trices (5.5) and (5.6) with a computational cost of  $O(mi^2)$  for the  ~~$i$ th~~ $i$ th eigenvector. Here, we have taken account of the sparse structure of (5.5) and (5.6). For a detailed discussion, see [16]. So, the total complexity of ~~the~~reordering method is approximately the same as that of one iteration in power iteration.


In summary, if we ~~only consider~~consider only the computational complexity, the combination of ~~periodic Schur decomposition~~algorithm and ~~the PSD algorithm and the~~reordering method is preferable for periodic eigendecomposition.

**7. Application to Kuramoto–Sivashinsky equation.** Our ultimate goal of implementing periodic eigendecomposition is to analyze the stability of periodic orbits and the associated stable/unstable manifolds in dynamical systems, ~~for in~~ the hope of getting a better understanding of pattern formation and turbulence. As an example, we focus on the one-dimensional Kuramoto–Sivashinsky equation

$$(7.1) \quad u_t + \frac{1}{2}(u^2)_x + u_{xx} + u_{xxxx} = 0, \quad x \in [0, L],$$



on a periodic spatial domain of size  $L = 22$ , large enough to exhibit complex spatiotemporal chaotic dynamics [8]. This equation is formulated independently by  ramoto in the context of angular phase turbulence in reaction-diffusion systems [22], and by Sivashinsky in the study of hydrodynamic instability in laminar flames [24]. ~~Periodic~~ periodic boundary condition




enables us to transform this ~~partial differential equation~~ PDE into a set of ODEs in Fourier space .

$$(7.2) \quad \dot{a}_k = (q_k^2 - q_k^4) a_k - i \frac{q_k}{2} \sum_{m=-\infty}^{\infty} a_m a_{k-m},$$

where  $q_k = 2\pi k/L$  and the coefficients are complex, i.e.  $a_k = b_k + ic_k$ . In our simulations, discrete Fourier transform is used with  $N = 64$  modes ( $k = -N/2 + 1$  up to  $N/2$  in (7.2)).

Since  $u(x, t)$  is real,  $a_k(t) = a_{-k}^*(t)$ ; thus, only half of the Fourier modes are independent. As  $\dot{a}_0 = 0$  from (7.2), we can set  $a_0 = 0$  corresponding to zero mean velocity without loss of generality. Also the nonlinear term   $\dot{a}_{N/2}$  in fact has coefficient  $-i(q_{N/2} + q_{-N/2})/2 = 0$  from symmetric consideration [30]; thus,  $a_{N/2}$  is decoupled from other modes, and it can be set to zero as well. ~~Thus, then~~ Then the number of independent variables is   $-2$ .

$$(7.3) \quad \hat{u} = (b_1, c_1, b_2, c_2, \dots, b_{N/2-1}, c_{N/2-1})^\top.$$

This is the ~~'state space'~~ "state space" in the discussion that follows. ~~Exponential~~ An exponential time-differencing scheme combined with  [4 [6, 19] is implemented to integrate (7.2). The combination of ~~periodic Schur decomposition algorithm and the~~ PSD algorithm and the re-ordering algorithm is used to obtain all exponents and eigenvectors. In addition, GEPP is stable for solving (5.5) and (5.6) if the time step in the Kuramoto-Sivashinsky integrator is not too large.

The Kuramoto-Sivashinsky equation is equivariant under reflection and space translation:  $-u(-x, t)$  and  $u(x+l, t)$  are also solutions if  $u(x, t)$  is a solution, which corresponds to equivariance of (7.3) under group operation  ~~$R = \text{diag}(-1, 1, -1, 1, \dots)$  and  $g(l) = \text{diag}(r_1, r_2, \dots, r_{N/2-1})$~~ , where  $R = \text{diag}(-1, 1, -1, 1, \dots)$  and  $g(l) = \text{diag}(r_1, r_2, \dots, r_{N/2-1})$ , where

$$r_k = \begin{pmatrix} \cos(q_k l) & -\sin(q_k l) \\ \sin(q_k l) & \cos(q_k l) \end{pmatrix}, \quad k = 1, 2, \dots, N/2 - 1.$$


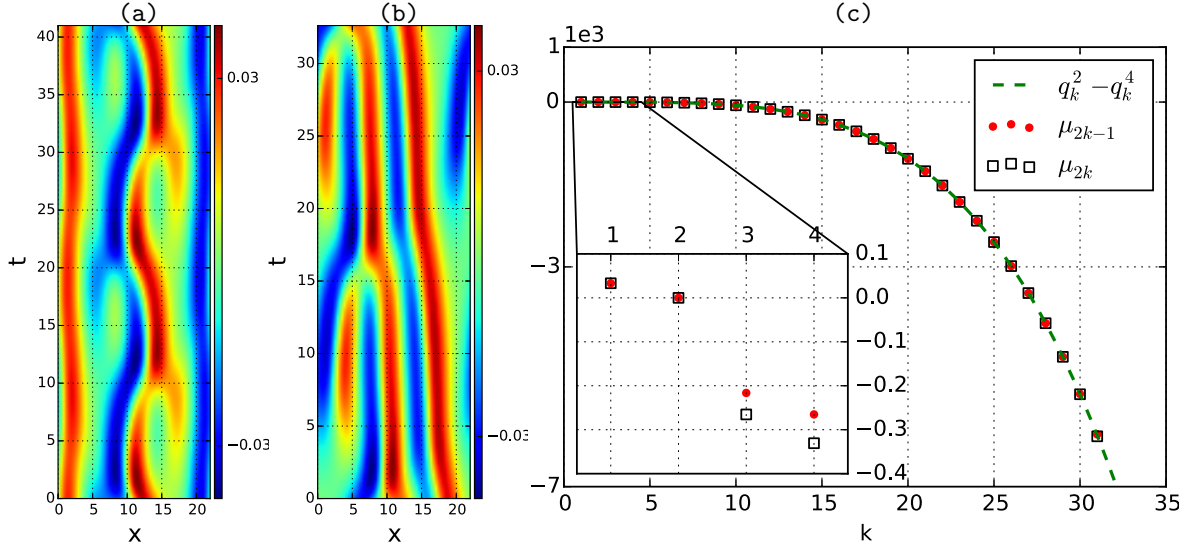
Based on the consideration of these symmetries, there are three types of invariant orbits in the Kuramoto-Sivashinsky system: periodic orbits in the  $b_k = 0$  invariant antisymmetric subspace, preperiodic orbits which are self-dual under reflection, and relative periodic orbits with a shift along  up orbit after one period. As shown in [8], the first type is absent for a domain as small as  $L = 22$ , and thus we focus on the last two types of orbits. For preperiodic orbits  $\hat{u}(0) = R\hat{u}(T_p)$ , we ~~only need to~~ need only evolve the system for a prime period  $T_p$  which is half of the whole period, with the Floquet matrix given by  $J_p(\hat{u}) = RJ^{T_p}(\hat{u})$ . A relative periodic orbit,  $\hat{u}(0) = g_p\hat{u}(T_p)$ , returns after one period  $T_p$  to the initial state upon the group transform  $g_p = g(l_p)$ , so the corresponding Floquet matrix is  $J_p(\hat{u}) = g_p J^{T_p}(\hat{u})$ . Here we show how periodic eigendecomposition works by applying it to one representative preperiodic orbit,  $\overline{pp}_{10.25}$ , and two relative periodic orbits,  $\overline{rp}_{16.31}$  and  $\overline{rp}_{57.60}$  (subscript indicates the period of the orbit), described in [8].

Figure 3 shows the time evolution of  $\overline{pp}_{10.25}$  and  $\overline{rp}_{16.31}$  and the Floquet spectrum of  $\overline{pp}_{10.25}$ . At each repeat of the prime period,  $\overline{pp}_{10.25}$  is invariant under reflection along  $x = L/2$ , ~~(a)~~ (Figure 3(a)), and  $\overline{rp}_{16.31}$  has a fixed shift along the  $x$  direction after each period, ~~(b)~~ (Figure 3(b)). Since  $\overline{pp}_{10.25}$  and  $\overline{rp}_{16.31}$  are both time invariant and equivariant under  $SO(2)$



**Figure 3.** (a) Preperiodic orbit  $\overline{pp}_{10.25}$  and (b) relative periodic orbit  $\overline{rp}_{16.31}$  for total evolution time  $T_{rp}$  and  $2T_{rp}$ , respectively. The spatial shift for  $\overline{rp}_{16.31}$  after one prime period  $\simeq -2.863$ . (c) The real parts of Floquet exponents paired for a given  $k$  as  $(k, \mu_{2k-1})$  and  $(k, \mu_{2k})$ , for  $\overline{pp}_{10.25}$  with truncation number  $N = 64$ . The dashed line (green) is  $q_k^2 - q_k^4$ . The inset is a magnification of the region containing the 8-eight leading exponents.

group transformation  $g(l)$ , there should be two marginal Floquet exponents, corresponding to the velocity field  $v(x)$  and group tangent  $t(x) = \mathbf{T}x$ , respectively, where  $\mathbf{T}$  is the generator of  $\text{SO}(2)$  rotation:

$$\mathbf{T} = \text{diag}(t_1, t_2, \dots, t_{N/2-1}), \quad t_k = \begin{pmatrix} 0 & -q_k \\ q_k & 0 \end{pmatrix}.$$

Table 1 shows that the 2<sup>nd</sup> and 3<sup>rd</sup> second and third, respectively, 3<sup>rd</sup> and 4<sup>th</sup> third and fourth, exponents of  $\overline{rp}_{16.31}$ , respectively,  $\overline{pp}_{10.25}$ , are marginal, with accuracy as low as  $10^{-12}$ , to which the inaccuracy introduced by the error in the closure of the orbit itself also contributes. Table 1 and Figure 3(c) show that periodic-Schur-decomposition PSD is capable of resolving Floquet multipliers differing by thousands of orders of magnitude: when  $N = 64$ , the smallest Floquet multiplier magnitude for  $\overline{pp}_{10.25}$  is  $|\Lambda_{62}| \simeq e^{-6080.4 \times 10.25}$ . This cannot be achieved if we try to compute a single Jacobian matrix for the whole orbit. Figure 3(c) and Table 1 also show that for large index  $k$ , Floquet exponents almost lie on the curve  $(q_k^2 - q_k^4)$ . This is the consequence of strong dissipation caused by the linear term in (7.2) for large Fourier mode index. Also, Floquet exponents appear in pairs for large indices simply because the real and complex parts of high Fourier modes have a similar contraction rate from (7.2).

Figure 4 shows a few selected Floquet vectors along  $\overline{pp}_{10.25}$  and  $\overline{rp}_{16.31}$  for one prime period, respectively. We need to remind the reader that Floquet vectors for a whole period are obtained by solving (5.5) or (5.6), not by evolving Floquet vectors at one time spot to the later time spots, because the evolution procedure is not stable for Floquet vectors. We can see that the leading few Floquet vectors have turbulent structures containing only long waves for both  $\overline{pp}_{10.25}$  and  $\overline{rp}_{16.31}$ , but for Floquet vectors corresponding to strong contraction rates,

Table 1

The first 10 and last four Floquet multipliers  $\Lambda_i = \exp(T\mu_i \pm i\theta_i)$  for orbits  $\overline{pp}_{10.25}$  and  $\overline{rp}_{16.31}$ , respectively. The  $\theta_i$  column lists either the phase  $\theta_i$  if the Floquet multiplier is complex, or  $\pm 1$  if the multiplier is real but inverse hyperbolic. ~~Truncation~~ The truncation number  $N = 64$ .

$\overline{pp}_{10.25}$			$\overline{rp}_{16.31}$		
$i$	$\mu_i$	$\theta_i$	$i$	$\mu_i$	$\theta_i$
1,2	0.033209	$\pm 2.0079$	1	0.32791	
3	<del>-4.1096</del> <del>-4.1096e-13</del>		2	2.8679e-12	
4	<del>-3.3524</del> <del>-3.3524e-14</del>	<del>-1</del>	3	2.3559e-13	
5	<del>-0.21637</del> <del>-0.21637</del>		4	<del>-0.13214</del> <del>-0.13214</del>	<del>-1</del>
6,7	<del>-0.26524</del> <del>-0.26524</del>	$\pm 2.6205$	5,6	<del>-0.28597</del> <del>-0.28597</del>	$\pm 2.7724$
8	<del>-0.33073</del> <del>-0.33073</del>	<del>-1</del>	7	<del>-0.32821</del> <del>-0.32821</del>	<del>-1</del>
9	<del>-1.9605</del> <del>-1.9605</del>		8	<del>-0.36241</del> <del>-0.36241</del>	
10	<del>-1.9676</del> <del>-1.9676</del>	<del>-1</del>	9,10	<del>-1.9617</del> <del>-1.9617</del>	$\pm 2.2411$
...	...	...	...	...	...
59	<del>-5313.6</del> <del>-5313.6</del>	<del>-1</del>	59	<del>-5314.4</del> <del>-5314.4</del>	
60	<del>-5317.6</del> <del>-5317.6</del>		60	<del>-5317.7</del> <del>-5317.7</del>	
61	<del>-6051.8</del> <del>-6051.8</del>	<del>-1</del>	61	<del>-6059.2</del> <del>-6059.2</del>	
62	<del>-6080.4</del> <del>-6080.4</del>		62	<del>-6072.9</del> <del>-6072.9</del>	

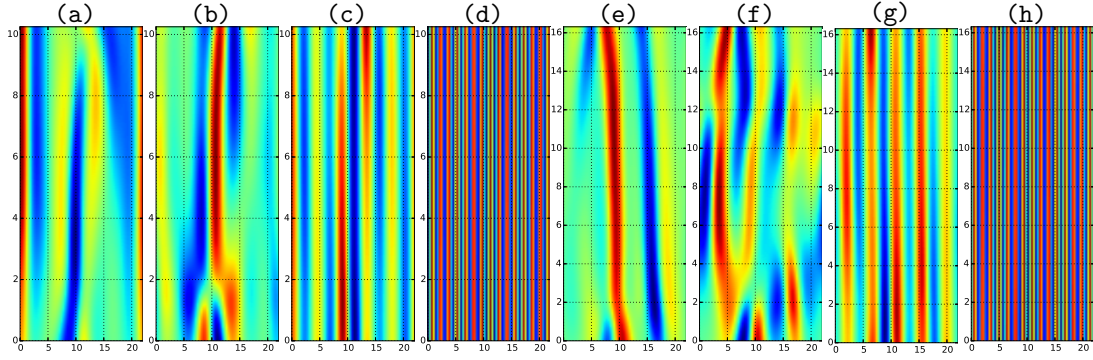
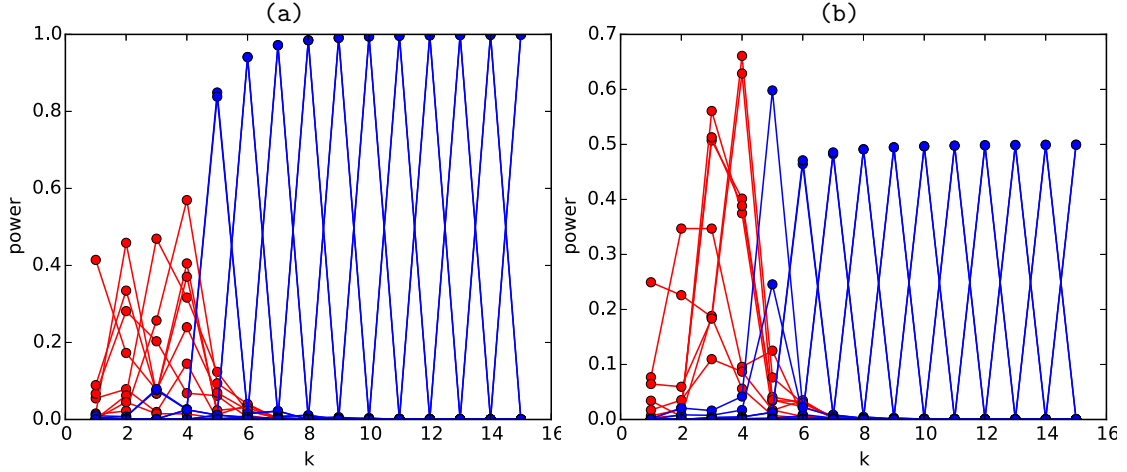


Figure 4. (Color-online) (a)–(d): the 1st (real part), 5th, 10th, and 30th Floquet vector along  $\overline{pp}_{10.25}$  for one prime period. (e)–(h): the 1st, 4th (real part), 10th (imaginary part), and 30th (imaginary part) Floquet vector along  $\overline{rp}_{16.31}$  for one prime period. Axes and color scale are the same as in Figure 3.

the configurations are pure sinusoidal curves. The power spectra in Figure 5 demonstrate this point, too. The leading 8-eight Floquet vectors have large components in the first 5-Fourier modes-five Fourier modes, and the spectra are entangled with each other, while the remaining Floquet vectors almost concentrate on a single Fourier mode and are decoupled from each other; more specifically, the  $i$ th Floquet vector with  $i \geq 9$  peaks at the  $\lceil \frac{i}{2} \rceil$ th<sup>3</sup> mode in Figure 5. Takeuchi et al. [27, 37] observe similar features in covariant Lyapunov vectors along ergodic trajectories, and by measuring the tangency between these two groups of covariant Lyapunov vectors, they reach a reasonable conclusion about the dimension of inertial manifold of the Kuramoto–Sivashinsky equation and complex Ginzburg–Landau equation. Therefore, we anticipate that analyzing the tangency of Floquet vectors along different periodic orbits

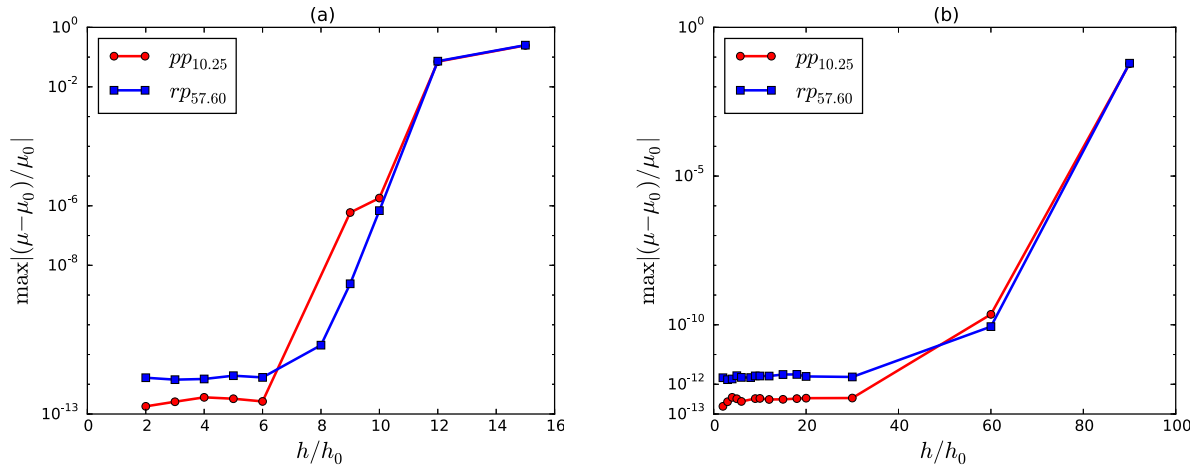
<sup>3</sup>Here,  $\lceil x \rceil$  denotes the smallest integer no less than  $x$ .



**Figure 5.** (Color online) The power spectrum of the first 30 Floquet vectors for  $\overline{p}p_{10.25}$  (left) and  $\overline{r}p_{16.31}$  (right) at  $t = 0$ . Red lines correspond to the leading 8 Floquet vectors, while the blue lines correspond to the left 22 Floquet vectors with the  $i$ -th one localized at index  $\lceil \frac{i}{2} \rceil$ . Power The power at index  $k$  is defined to be as the square of the  $k$ -th Fourier coefficient's magnitude of Floquet vectors. The x-axis is labeled by the Fourier mode indices. Only the  $k > 0$  part is shown, and the part for negative  $k$  follows by reflection. For complex Floquet vectors, the power spectra of the real part and the imaginary part are calculated separately. Since almost all contracting Floquet vectors of  $\overline{r}p_{16.31}$  form complex conjugate pairs, their power peaks are far less than 1, as shown in panel (b).

can also lead to the same conclusion, which is goal of our future research.

We have noted above that the semi-group semigroup property of Jacobian matrix (2.1) enables us to factorize  $\mathbf{J}^{(k)}$  into a product of short-time matrices with matrix elements of comparable order of magnitude. In practice, caution should be exercised when trying to determine the optimal number of time increments that into which the orbit should be divided into. If the number of time increments  $m$  is too large, then, according to the estimates of sect. 6 section 6, the computation may be too costly. If  $m$  is too small, then the elements of the Jacobian matrix corresponding to the corresponding time increment may range over too many orders of magnitude, causing periodic eigendecomposition to fail to resolve the most contracting Floquet vector along the orbit. One might also vary the time step according to the velocity at a given point on the orbit. Here we determined satisfactory  $m$ 's by numerical experimentation shown in Since Figure 6. Since a larger time step means fewer time increments of the orbit, a very small time step ( $h_0 \approx 0.001$ ) is chosen as the base case, and it is increased to test whether the corresponding Floquet exponents change substantially or not. As shown in Figure 6(a), up to  $6h_0$  the whole Floquet spectrum varies within  $10^{-12}$  for both  $\overline{p}p_{10.25}$  and  $\overline{r}p_{57.60}$ . These two orbits represent two different types of invariant solutions which have short and long periods, respectively, so we presume that time step  $6h_0$  is good enough for other short or long orbits, too. On the other hand, if only the first few Floquet exponents are desired, the time step can be increased further to fulfill the job. As shown in Figure 6(b), if we are only interested in interested in only the first 35 Floquet exponents, then time step  $30h_0$  is small enough. In high-dimensional high-dimensional nonlinear systems, often we are not interested in very contracting directions because the dynamics in these directions are transient and shed little

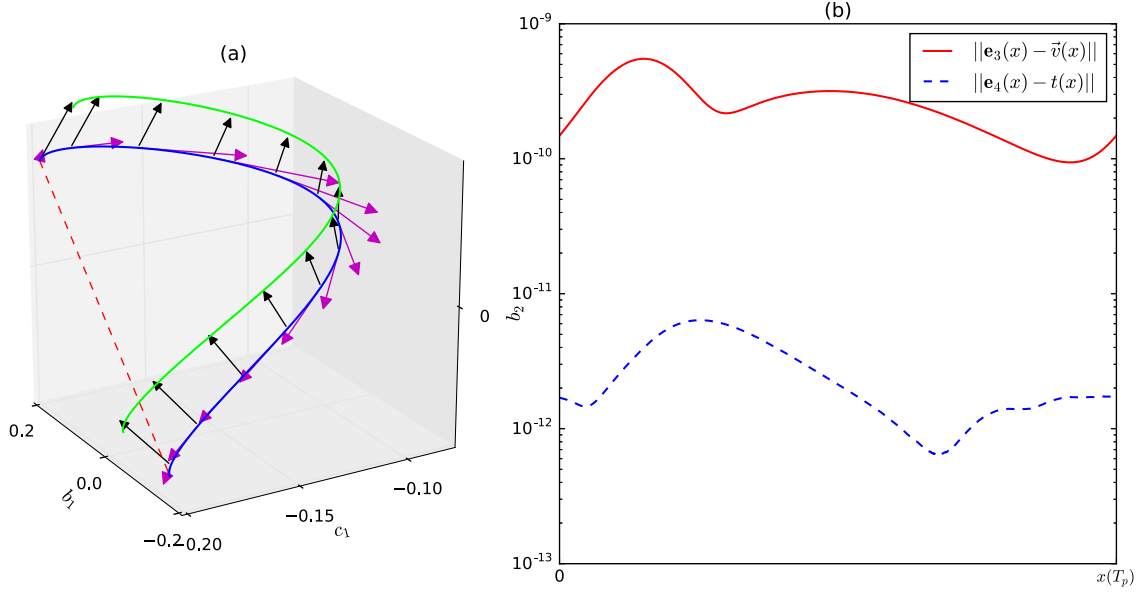


**Figure 6.** (Color online) Relative error of the real part of Floquet exponents associated with different time steps with which the Floquet matrix is integrated. Two orbits  $pp_{10.25}$  and  $rp_{57.60}$  are used as an example with the base case  $h_0 \approx 0.001$ . (a) The maximal relative difference of the whole set of Floquet exponents with increasing time step (decreasing the number of ingredient segments of the orbit). (b) ~~Only consider~~ Consider only the first 35 Floquet exponents.


insight into the system properties. Therefore, a large time step could be used to save time.


The two marginal directions have a simple geometrical interpretation and provide a metric for us to measure the convergence of periodic eigendecomposition. Figure 7(a) depicts the two marginal vectors of  $pp_{10.25}$  projected onto the subspace spanned by  $[b_1, c_1, b_2]$  (the real and imaginary parts of the first mode and the real part of the second Fourier mode). The first marginal direction (the ~~3rd~~ third Floquet vector in Table 1) is aligned with the velocity field along the orbit, and the second marginal direction (the ~~4th~~ fourth Floquet vector) is aligned with the group tangent. The numerical difference between the unit vectors along these two marginal directions and the corresponding physical directions is shown in Figure 7(b). The difference is ~~under~~ less than  $10^{-9}$  and  $10^{-11}$  for these two directions, which demonstrates the accuracy of the algorithm. As shown in Table 1, for a preperiodic orbit, such as  $pp_{10.25}$ , the velocity field and the group tangent have eigenvalue  $+1$  and  $-1$ , respectively, and are thus distinct. However, the two marginal directions are degenerate for a relative periodic orbit, such as  $rp_{16.31}$ . So these two directions are not fixed, but the ~~two-dimensional~~ two-dimensional plane spanned by them is uniquely determined. Figure 8 shows that the velocity field and group tangent along orbit  $rp_{16.31}$  indeed lie in the subspace spanned by these two marginal directions.

**8. Conclusion and future work.** In this paper, we use the one-dimensional Kuramoto-Sivashinsky system to illustrate the effectiveness and potential wide usage of periodic eigendecomposition applied to stability analysis in dissipative nonlinear systems. On the longer time scale, we hope to apply the method to the study of orbits of much longer periods, as well as to the study of high-dimensional, numerically exact time-recurrent unstable solutions of the full ~~Navier-Stokes~~ Navier-Stokes equations. Currently, up to 30 Floquet vectors for plane Couette invariant solutions can be computed [12], but many more will be needed and to




**Figure 7.** (Color-online) Marginal vectors and the associated errors. (a)  $\overline{pp}_{10.25}$  in one period projected onto the  $[b_1, c_1, b_2]$  subspace (blue curve), and its counterpart (green line) generated by a small group transformation  $g(\ell)$ , here arbitrarily set to  $\ell = L/(20\pi)$ . Magenta and black arrows represent the first and the second marginal Floquet vectors  $\mathbf{e}_3(x)$  and  $\mathbf{e}_4(x)$  along the prime orbit. (b) The solid red curve is the Euclidean difference between  $\mathbf{e}_3(x)$  and the velocity field  $\vec{v}(x)$  along the orbit, and the blue dashed curve is the difference between  $\mathbf{e}_4(x)$  and the group tangent  $t(x) = \mathbf{T}x$ .

a higher accuracy in order to determine the physical dimension of a turbulent **Navier-Stokes** **Navier-Stokes** flow.  are nowhere ~~there~~ near achieving this yet; we anticipate the need for optimizing and parallelizing such algorithms. Also, there is an opportunity to apply periodic eigendecomposition to Hamiltonian systems, and we need additional tests to show its ability to preserve symmetries of the Floquet spectrum imposed by Hamiltonian systems.

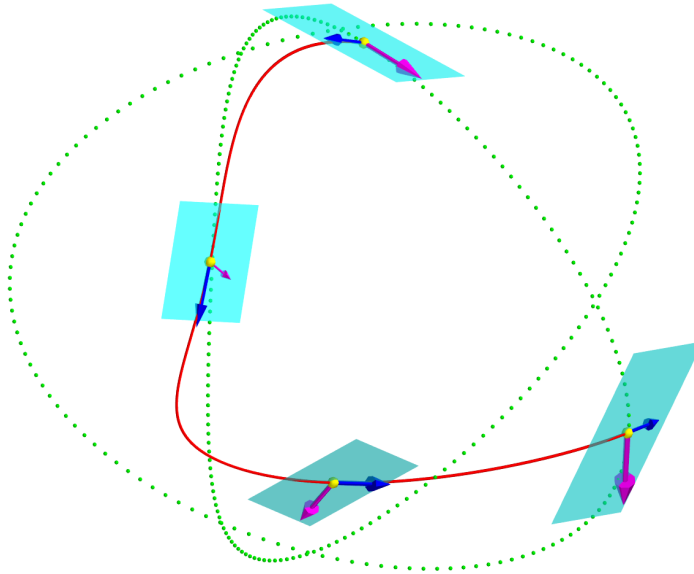
**Acknowledgments.** We are grateful to L. Dieci for introducing us to complex periodic Schur decomposition, K.A. Takeuchi for providing detailed documentation of his previous work on covariant Lyapunov vectors, R.L. Davidchack for his database of periodic orbits in the Kuramoto–Sivashinsky equation, which is the basis of our numerical experiments, and ~~to~~ N.B. Budanur, E. Siminos, M.M. Farazmand, and H. Chaté for many spirited exchanges. P.C. thanks G. Robinson, Jr.  support.

## REFERENCES



- [1] P. AMODIO, J. R. CASH, G. ROUSSOS, R. W. WRIGHT, G. FAIRWEATHER, I. GLADWELL, G. L. KRAUT, AND M. PAPRZYCKI, *Almost block diagonal linear systems: Sequential and parallel solution techniques, and applications*, Numer. Linear Algebra Appl., 7 (2000), pp. 275–317.
-  [2] G. BENETTIN, L. GALGANI, A. GIORGILLI, AND J. ~~M.M.~~ STRELCYN, *Lyapunov characteristic exponents for smooth dynamical systems and for Hamiltonian systems; a method for computing all of them. Part 1: Theory*, Meccanica, 15 (1980), pp. 9–20.
- [3] A. BOJANCZYK, G. H. GOLUB, AND P. ~~V.-VAN~~ DOOREN, *The periodic Schur decomposition. Algo-*





**Figure 8.** (Color online) Projection of relative periodic orbit  $\bar{r}p_{16.31}$  onto the Fourier modes subspace  $[b_2, c_2, b_3]$  (red curve). The dotted curve is the group orbit connecting the initial and final points. Blue and magenta arrows represent the velocity field and the group tangent along the orbit, respectively. Two-dimensional planes (cyan) are spanned by the two marginal Floquet vectors at each point (yellow) along the orbit.

rhythms and applications, in Proc. SPIE Conference, vol. 1770, [Advanced Signal Processing Algorithms, Architectures, and Implementations III](#), SPIE, Bellingham, WA, 1992, pp. 31–42.

- [4] H. BOSETTI, H. A. POSCH, C. DELLAGO, AND W. G. HOOVER, *Time-reversal symmetry and covariant Lyapunov vectors for simple particle models in and out of thermal equilibrium*, Phys. Rev. E, 82 (2010), pp. 1–10.
- [5] F. CHRISTIANSEN, P. CVITANOVIĆ, AND V. PUTKARADZE, *Hopf’s last hope: Spatiotemporal chaos in terms of unstable recurrent patterns*, Nonlinearity, 10 (1997), pp. 55–70.
- [6] S. M. COX AND P. C. MATTHEWS, *Exponential time differencing for stiff systems*, J. Comput. Phys., 176 (2002), pp. 430–455.
- [7] P. CVITANOVIĆ, R. ARTUSO, R. MAINIERI, G. TANNER, AND G. VATTAY, *Chaos: Classical and Quantum*, Niels Bohr Institute, Copenhagen, 2016.
- [8] P. CVITANOVIĆ, R. L. DAVIDCHACK, AND E. SIMINOS, *On the state space geometry of the Kuramoto-Sivashinsky flow in a periodic domain*, SIAM J. Appl. Dyn. Syst., 9 (2010), pp. 1–33, doi:10.1137/070705623.
- [9] S. V. ERSHOV AND A. B. POTAPOV, *On the concept of stationary Lyapunov basis*, Physica Phys. D, 118 (1998), pp. 167–198.
- [10] G. FAIRWEATHER AND I. GLADWELL, *Algorithms for almost block diagonal linear systems*, SIAM Rev., 46 (2004), pp. 49–58, doi:10.1137/S003614450240506X.
- [11] J. G. F. FRANCIS, *The QR transformation: A unitary analogue to the LR transformation. I*, Comput. J., 4 (1961/1962), pp. 265–271.
- [12] J. F. GIBSON, J. HALCROW, AND P. CVITANOVIĆ, *Visualizing the geometry of state-space in plane Couette flow*, J. Fluid Mech., 611 (2008), pp. 107–130.
- [13] F. GINELLI, H. CHATÉ, R. LIVI, AND A. POLITI, *Covariant Lyapunov vectors*, J. Phys. A, 46 (2013), p. 254005.
- [14] F. GINELLI, P. POGGI, A. TURCHI, H. CHATÉ, R. LIVI, AND A. POLITI, *Characterizing dynamics with*

- covariant Lyapunov vectors, Phys. Rev. Lett., 99 (2007), ~~p-130601;~~ [130601](#).
- [15] R. GRANAT, I. JONSSON, AND B. KÅGSTRÖM, *Recursive blocked algorithms for solving periodic triangular Sylvester-type matrix equations*, in ~~Proceedings of the 8th International Conference of Applied Parallel Computing: State of the Art in Scientific Computing, PARA'06, 8th International Workshop, PARA 2006, Springer-Verlag, Berlin, Heidelberg~~, 2007, pp. 531–539.
- [16] R. GRANAT AND B. KÅGSTRÖM, *Direct eigenvalue reordering in a product of matrices in periodic Schur form*, SIAM J. Matrix Anal. Appl., 28 (2006), pp. 285–300, [doi:10.1137/05062490X](#).
- [17] J. GUCKENHEIMER AND P. HOLMES, *Nonlinear Oscillations, Dynamical Systems, and Bifurcations of Vector Fields*, Springer, New York, 1983.
- [18] M. INUBUSHI, M. U. KOBAYASHI, S. ~~+~~[I](#). TAKEHIRO, AND M. YAMADA, *Covariant Lyapunov analysis of chaotic Kolmogorov flows*, Phys. Rev. E, 85 (2012), ~~p-~~016331.
- [19] A.-K. KASSAM AND L. N. TREFETHEN, *Fourth-order ~~time-stepping~~ time-stepping for stiff PDEs*, SIAM J. Sci. Comput., 26 (2005), pp. 1214–1233, [doi:10.1137/S1064827502410633](#).
- [20] P. V. KUPTSOV, *Violation of hyperbolicity via unstable dimension variability in a chain with local hyperbolic chaotic attractors*, J. Phys. A, 46 (2013), ~~p-~~254016.
- [21] P. V. KUPTSOV AND U. PARLITZ, *Theory and computation of ~~Covariant-covariant~~ Lyapunov ~~Vectors-vectors~~*, J. ~~Nonlin-~~Nonlinear Sci., 22 (2012), pp. 727–762; ~~-~~.
- [22] Y. KURAMOTO AND T. TSUZUKI, *On the formation of dissipative structures in ~~reaction-diffusion~~ reaction-diffusion systems*, ~~Prog-Theor~~Progr. Theoret. Phys., 54 (1975), pp. 687–699.
- [23] K. LUST, *Improved numerical Floquet multipliers*, ~~Int~~Internat. J. Bifur. Chaos [Appl. Sci. Engrg.](#), 11 (2001), pp. 2389–2410.
- [24] D. M. MICHELSON AND G. I. SIVASHINSKY, *Nonlinear analysis of hydrodynamic instability in laminar ~~flames-flames~~-II. Numerical experiments*, Acta Astronaut., 4 (1977), pp. 1207–1221.
- [25] V. I. OSELEDEC, *A multiplicative ergodic theorem. Liapunov characteristic numbers for dynamical systems*, Trans. Moscow Math. Soc., 19 (1968), pp. 197–221.
- [26] D. RUELLE, *Ergodic theory of differentiable dynamical systems*, [Inst. Hautes Études Sci. Publ. Math.](#)~~HES~~, 50 (1979), pp. 27–58.
- [27] K. A. TAKEUCHI, H. YANG, F. GINELLI, G. RADONS, AND H. CHATÉ, *Hyperbolic decoupling of tangent space and effective dimension of dissipative systems*, Phys. Rev. E, 84 (2011), ~~p-046214;~~ [046214](#).
- [28] R. TEMAM, *Inertial manifolds*, Math. ~~Intell~~Intelligencer, 12 (1990), pp. 68–74.
- [29] R. TEMAM, *Infinite-Dimensional Dynamical Systems in Mechanics and Physics*, 2nd ed., Springer, New York, 2013.
- [30] L. N. TREFETHEN, *Spectral Methods in MATLAB*, [Software, Environ. Tools 10](#), SIAM, Philadelphia, ~~2000-~~2000, [doi:10.1137/1.9780898719598](#).
- [31] L. N. TREFETHEN AND D. BAU, [III](#), *Numerical Linear Algebra*, SIAM, Philadelphia, 1997.
- [32] D. S. WATKINS, *The Matrix Eigenvalue Problem: GR and Krylov Subspace Methods*, SIAM, Philadelphia, ~~2007-~~2007, [doi:10.1137/1.9780898717808](#).
- [33] D. S. WATKINS, *Francis's algorithm*, Amer. Math. Monthly, 118 (2011), pp. 387–403.
- [34] C. L. WOLFE AND R. M. SAMELSON, *An efficient method for recovering Lyapunov vectors from singular vectors*, Tellus A, 59 (2007), pp. 355–366.
- [35] H. YANG AND G. RADONS, *Geometry of inertial manifold probed via Lyapunov projection method*, Phys. Rev. Lett., 108 (2012), ~~p-~~154101.
- [36] H. ~~+~~[L](#). YANG AND G. RADONS, *Comparison between covariant and orthogonal Lyapunov vectors*, Phys. Rev. E [\(3\)](#), 82 (2010), ~~p-046204;~~ [046204](#).
- [37] H. ~~+~~[L](#). YANG, K. A. TAKEUCHI, F. GINELLI, H. CHATÉ, AND G. RADONS, *Hyperbolicity and the effective dimension of ~~spatially-extended~~ spatially extended dissipative systems*, Phys. Rev. Lett., 102 (2009), ~~p-074102;~~ [074102](#).